Inorganic Chemistry

Article

pubs.acs.org/IC

Design of a Catalytic Active Site for Electrochemical CO_2 Reduction with Mn(I)-Tricarbonyl Species

Jay Agarwal,[†,‡,§] Travis W. Shaw,[‡,§] Henry F. Schaefer, III,[†] and Andrew B. Bocarsly*[,‡]

[†]Center for Computational Quantum Chemistry, University of Georgia, Athens, Georgia 30602, United States

[‡]Department of Chemistry, Princeton University, Princeton, New Jersey 08544, United States

Supporting Information

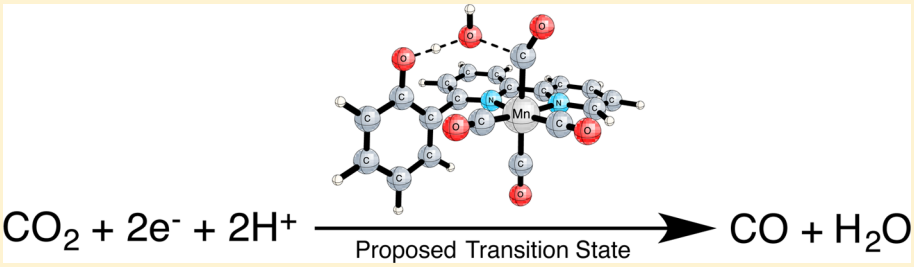

ABSTRACT: The design, synthesis, and assessment of a new manganese-centered catalyst for the electrochemical reduction of CO_2 is described. The reported species, MnBr(6-(2-hydroxyphenol)-2,2′-bipyridine)$(CO)_3$, includes a ligand framework with a phenolic proton in close proximity to the CO_2 binding site, which allows for facile proton-assisted C−O bond cleavage. As a result of this modification, seven times the electrocatalytic current enhancement is observed compared to MnBr(2,2′-bipyridine)$(CO)_3$. Moreover, reduction is possible at only 440 mV of overpotential. Theoretical computations suggest that the entropic contribution to the activation free energy is partially responsible for the increased catalytic activity. Experimental work, including voltammetry and product quantification from controlled potential electrolysis, suggests a key mechanistic role for the phenolic proton in the conversion of CO_2 to CO.

INTRODUCTION

Carbon dioxide (CO_2) is an abundant and inexpensive chemical that is appealing as a C1 building block for producing fuels.[1] Yet, the efficient utilization of CO_2 as a feedstock remains a challenge in fundamental energy research. Progress in this area has been hindered, in part, by the extremely stable nature of CO_2, and the lack of selective materials for effectively storing and/or transferring multiple redox equivalents. One promising solution is the electrocatalytic reduction of CO_2 using metal-based catalysts. This approach is especially attractive for electrical energy load-leveling, which is necessary for the pragmatic utilization of intermittent energy sources such as wind or solar. For this to be possible, efficient and selective electrocatalysts for use on the industrial scale must be developed.

The electrochemical reduction of CO_2 has been the focus of research for decades, and both heterogeneous[2−4] and homogeneous[5−10] catalysts have been investigated in this context. Our focus is on recently developed manganese(I)-tricarbonyl catalysts of the form MnX(κ^2-L)$(CO)_3$, where X is often a halogen and κ^2-L is a bidentate ligand such as 2,2′-bipyridine (bpy).[11−17] MnBr(bpy)$(CO)_3$ was originally reported to be electrocatalytic for the reduction of CO_2 to CO by Bourrez and co-workers, based on an observed turnover number (TON) of 13, and a recorded catalytic current enhancement under a CO_2 atmosphere.[11] This complex, along with related compounds where κ^2-L is varied, displays excellent selectivity for the two-electron reduction of CO_2 to CO, and offers several improvements over well-known Re(I)-tricarbonyl analogues.[18−25] Namely, the two-electron reduction potential is shifted anodic—providing improved energy efficiency—and, as an Earth-abundant metal, the starting material [MnX$(CO)_5$] is less expensive. Notwithstanding this progress, additional improvements are needed to increase the energy efficiency for use on the industrial scale.

To that end, several groups have investigated routes to optimize and improve the activity of manganese-based catalysts through modification of the first and second coordination sphere, as well as by adjusting the catalysis environment. Examples of the former include work by Kubiak and co-workers who substituted the 4- and 4′-positions of bpy with *tert*-butyl, yielding MnBr(4,4′-di-*tert*-butyl-bpy)$(CO)_3$,[12] or the replacement of bipyridine with terpyridine, which was reported earlier this year by Compain and co-workers.[15] We previously investigated the substitution of one pyridyl in bpy with an *N*-heterocyclic carbene (NHC).[17]

Both Ishitani and Kubiak have separately reported modifications of the catalytic environment. Ishitani and co-workers reported the use of a Ru$(bpy)_3^{2+}$ photosensitizer in combination with a MnBr(bpy)$(CO)_3$ electrocatalyst to produce CO and HCOOH from CO_2,[14] and Kubiak and co-

Received: February 4, 2015
Published: May 13, 2015

DOI: 10.1021/acs.inorgchem.5b00233
Inorg. Chem. 2015, 54, 5285−5294

workers reported that the addition of Brønsted acids, such as methanol and trifluoroethanol, can dramatically increase the catalytic current density.[12] Their investigation on the addition of acids builds from previous studies with Re(I)-tricarbonyl catalysts,[21,26] and, even earlier, from the work of Savéant and co-workers, who reported the use of Brønsted acids for CO_2 reduction using iron-porphyrin catalysts.[27,28]

Further improvements for manganese catalysts may be realized by considering the addition of noninnocent functional groups in the second coordination sphere.[29,30] Such an approach was utilized in related work by DuBois and co-workers, who installed a positive phosphonium group to stabilize CO_2 molecules coordinated to Pd- and Ni-based catalysts.[31] Additional catalytic current enhancement was observed in binuclear palladium catalysts where one metal center was available to coordinate the C atom of CO_2 and another, distal metal center could bind one of the O atoms.[32] In 2007, Jeoung and Dobbek reported that the binuclear stabilization of CO_2 also occurs within the Ni,Fe-cluster of carbon monoxide dehydrogenase, which reversibly oxidizes CO to CO_2.[33] And, more recently, Savéant and co-workers noted that the inclusion of ancillary phenolic groups on their iron porphyrin catalysts also yielded current enhancement at the potential of CO_2 reduction.[34,35] The authors suggested that the use of phenolic ligands introduces a greater local concentration of acid than would be possible to realize by adding acid to the electrolyte solution. These protons act as the oxide acceptor for the conversion of CO_2 to CO and H_2O.

In the present work, we have aimed to design an active site for CO_2 coordination based on MnBr(bpy)$(CO)_3$. To that end, we have installed a pendant phenolic group in the second coordination sphere with the intention of directly stabilizing the O atom of CO_2 through hydrogen bonding. Our approach is summarized in Figure 1, where we compare hydrogen-bonding

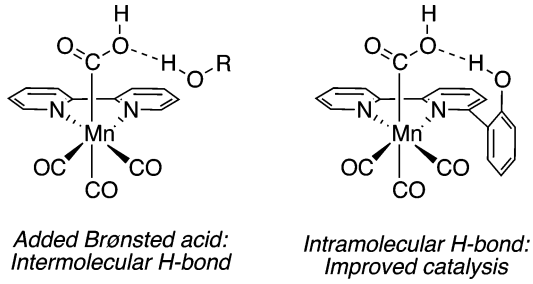

Figure 1. Intramolecular hydrogen bonding as a strategy for improved catalysis in CO_2 reduction.

from a solvent donor to the internal bond designed into the molecule. Notably, using cyclic voltammetry, we observe an improved catalytic current enhancement and a reduced overpotential using this phenol-substituted manganese catalyst over the parent complex, even with the presence of an added Brønsted acid. Further experimental work is presented to confirm our hypothesis through linear sweep voltammetry and product quantification from controlled potential electrolysis. We also utilize theory to investigate several mechanisms for CO production from a suggested Mn(N–N)$(CO)_3$COOH intermediate. Analysis of the entropic contribution to the free energies provides evidence for our mechanistic rationale for the improved catalytic activity of this complex.

RESULTS AND DISCUSSION

We began by extending the 2,2′-bipyridine framework at the 6-position with phenol to form 6-(2-hydroxyphenyl)-2,2′-bipyridine (HOPh-bpy).[36] The respective manganese complex, MnBr(HOPh-bpy)$(CO)_3$ (**1**), was then prepared by refluxing equimolar amounts of ligand (HOPh-bpy) and $MnBr(CO)_5$ in methanol under an argon atmosphere for 1 h. Compound **1** was characterized by nuclear magnetic resonance (^{1}H NMR and ^{13}C NMR) and Fourier transform infrared (FT-IR) spectroscopy. Crystals suitable for single-crystal X-ray analysis were obtained from the slow diffusion of hexanes into a solution of **1** in DCM/THF (see Figure 2).

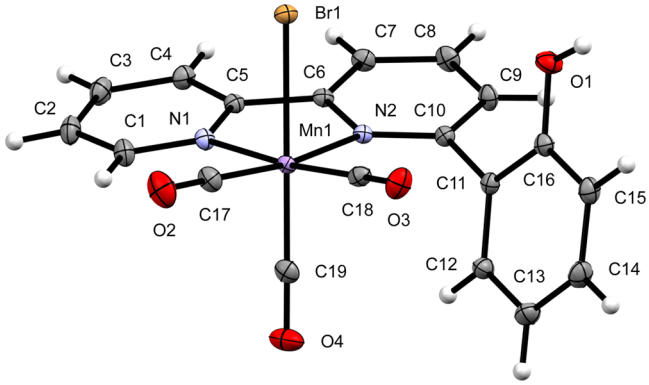

Figure 2. X-ray crystal structure of MnBr(HOPh-bpy)$(CO)_3$ (**1**) with ellipsoids set at 50% probability.

The cyclic voltammetry of **1** under argon in MeCN with 5% H_2O shows three reduction waves (Figure 3, inset): two waves spaced 160 mV apart that occur at −1.14 V and −1.30 V versus the saturated calomel electrode (SCE), and a third wave that appears at −1.76 V vs SCE. The first reduction wave corresponds to a metal-based reduction of the Mn center, which leads to the formation of a Mn–Mn dimer.[37] In MnBr(bpy)$(CO)_3$, oxidative cleavage of the metal–metal bond within the corresponding dimer is observed at −0.30 V vs SCE.[12] We similarly find an oxidative wave for this process at ca. −0.4 V vs SCE. The second reduction wave at −1.30 V vs SCE is composed of two overlapping waves spaced 30 mV apart and appears quasi-reversible.

To gauge the electrolytic stability of complex **1** and MnBr(bpy)$(CO)_3$, 15 μmol (1 mM) of each were separately electrolyzed at −1.5 V vs SCE under an argon atmosphere for 4 h. Over this period of time, we observed between 3 and 6.5 μmol of CO via gas chromatography (GC), indicating limited evolution of CO from either compound. Note that the loss of all three CO ligands would have resulted in the detection of 45 μmol of CO. Comparable CO loss among **1** and MnBr(bpy)-$(CO)_3$ indicates that the phenolic modification does not impart instability.

Under an atmosphere of CO_2, **1** displays significant current enhancement—an 11-fold increase from 0.58 mA/cm^2 to 6.3 mA/cm^2—at the potential of the second reduction (see Figure 3, red trace). The observed current enhancement for **1** is roughly seven times greater than that observed for MnBr-(bpy)$(CO)_3$ (see page S18 in the Supporting Information). Furthermore, a plot of the current function versus the scan rate at −1.5 V vs SCE is consistent with a catalytic mechanism as defined by Nicholson and Shain (see page S16 in the Supporting Information).[38] After electrolyzing 15 μmol (1

DOI: 10.1021/acs.inorgchem.5b00233
Inorg. Chem. 2015, 54, 5285–5294

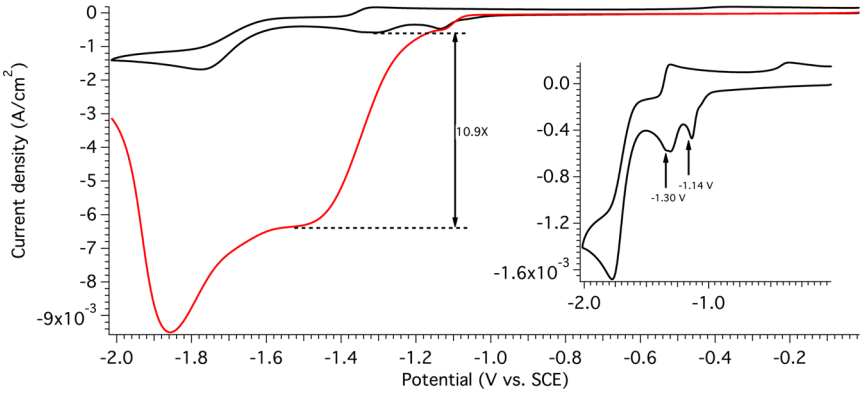

Figure 3. Cyclic voltammogram of MnBr(HOPh-bpy)$(CO)_3$ (**1**) under argon (black trace, also see inset) and CO_2 (red trace) at 100 mV s^{-1} (for additional scan rates, see pages S13 and S15 in the Supporting Information) in CH_3CN with 0.1 M tetrabutylammonium perchlorate (TBAP) as the supporting electrolyte and 5% water. The complex was loaded at a concentration of 1 mM. The proton content was kept constant under argon and CO_2.

mM) of **1** under CO_2 for 4 h, we detected 44.5 μmol of CO (see Figure 4). Considering the minimal CO evolution under

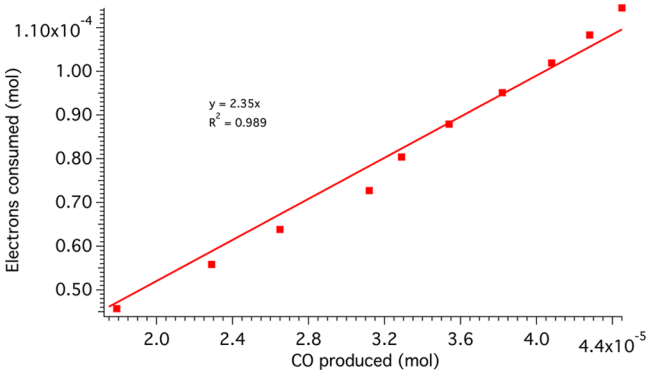

Figure 4. Production of CO from CO_2 by **1** during bulk electrolysis. The average Faradaic efficiency of **1** was 76%. Data were collected at −1.5 V vs SCE with solutions of the complex (1 mM) loaded in CO_2-saturated CH_3CN with 0.1 M tetrabutylammonium perchlorate (TBAP) as the supporting electrolyte and water (5%).

an argon atmosphere for the same time period (see page S21 in the Supporting Information), ∼40 μmol may be attributed to catalytic conversion, yielding a TON of 2.7. The linear relationship between the number of electrons consumed further supports catalysis, since decomposition should favor a nonlinear response.

To further confirm catalysis, **1** and MnBr(bpy)$(CO)_3$ were separately electrolyzed under an atmosphere of $^{13}CO_2$ at −1.5 V vs SCE, yielding both ^{13}CO and ^{12}CO in the head space of the electrolysis cell (see pages S19 and S20 in the Supporting Information). This is the first use of isotope labeling to confirm CO_2 conversion to CO using the parent complex, MnBr(bpy)-$(CO)_3$. We note that the presence of ^{12}CO is expected: a probable pathway for CO_2 reduction (discussed in the Theory section) is the formation of a Mn−COOH moiety after CO_2 coordination, and subsequent cleavage of the hydroxyl group to yield Mn−CO, which dissociates to evolve CO. Under $^{13}CO_2$, a $[Mn(N{-}N)(^{12}CO)_3\ ^{13}CO]^+$ intermediate would result, which could yield either ^{12}CO or ^{13}CO from axial ligand dissociation.

Based on these labeling experiments and literature precedent for both Mn(I)- and Re(I)-tricarbonyl catalysts,[12,17,21] we assign the reduction wave for **1** at −1.30 V vs SCE to the generation of the catalytically active species: $[Mn(HOPh\text{-}bpy)(CO)_3]^-$. This reactive intermediate possesses a vacant axial site for the coordination and reduction of CO_2. We attribute the third process at −1.76 V vs SCE to the reduction of available phenolic protons in close proximity to the metal center. Scan rate dependence data were obtained for **1** at scan rates between 50 mV s^{-1} and 1000 mV s^{-1} (see pages S13 and S15 in the Supporting Information). Consistent with other reported manganese catalysts, the peak current at the potential of the second reduction is proportional to the square root of the scan rate, indicating a diffusion-controlled process.

Encouraged by the voltammetric response observed for **1** under CO_2, we sought to verify that the presence of a phenolic proton in the second coordination sphere was indeed responsible for the large catalytic current enhancement. To that end, we synthesized a 2,2′-bipyridine ligand that was derivitized at the 6-position with anisole: 6-(2-methoxyphenyl)-2,2′-bipyridine (MeOPh-bpy).[36] The corresponding manganese complex MnBr(MeOPh-bpy)$(CO)_3$ (**2**) was obtained using the same synthesis as **1** and similarly characterized. Crystals suitable for single-crystal X-ray analysis were obtained from the slow diffusion of hexanes into a solution of **2** in DCM (see Figure 5).

The cyclic voltammetry of **2** under argon in MeCN with 5% H_2O is shown in Figure 6 (black trace). Only two reduction waves are observed, separated by 90 mV. The first reduction

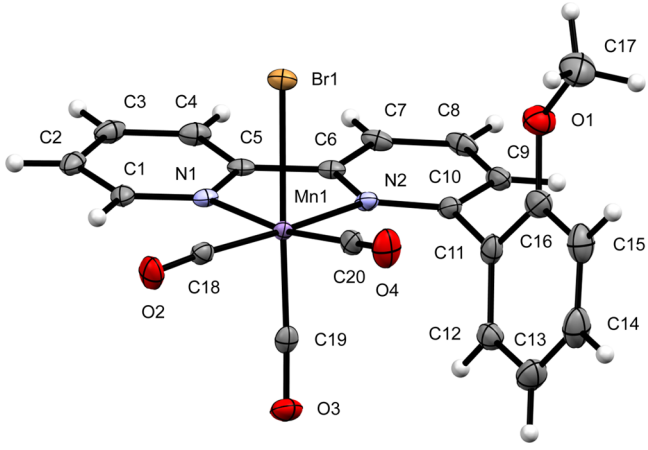

Figure 5. X-ray crystal structure of MnBr(MeOPh-bpy)$(CO)_3$ (**2**) with ellipsoids set at 50% probability.

DOI: 10.1021/acs.inorgchem.5b00233
Inorg. Chem. 2015, 54, 5285−5294

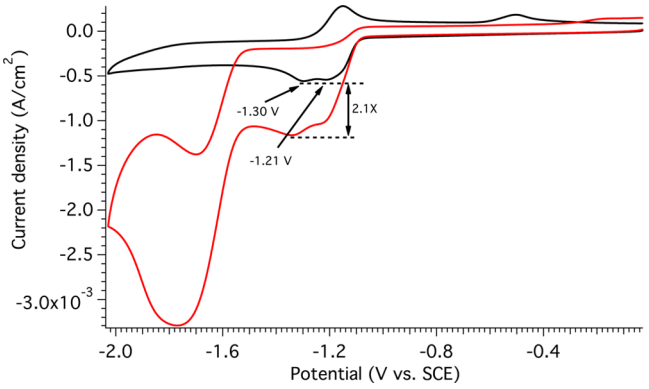

Figure 6. Cyclic voltammogram of MnBr(MeOPh-bpy)$(CO)_3$ (**2**) under argon (black trace) and CO_2 (red trace) at 100 mV s^{-1} (for additional scan rates, see page S17 in the Supporting Information) in CH_3CN with 0.1 M tetrabutylammonium perchlorate (TBAP) as the supporting electrolyte and 5% water. The complex was loaded at a concentration of 1 mM. The proton content was kept constant under argon and CO_2.

wave at −1.21 V vs SCE is shifted cathodic by 70 mV, compared to the same wave for **1**, while the second wave occurs at the same voltage, −1.30 V vs SCE. The wave previously assigned to oxidative cleavage of the Mn−Mn bond in the dimer that forms after one electron reduction appears at ca. −0.5 V vs SCE. Under CO_2 (red trace), the current enhancement, relative to the Ar scan at the potential of the second reduction, is 2.1×, which is marginally higher than the increase observed for MnBr(bpy)$(CO)_3$ (1.6×). These data strongly suggest that indeed a phenolic proton is required in order to effect significant current increase, but it does not indicate whether the same effect could be achieved by the addition of phenol to the electrolyte solution.

To determine if the incorporation of phenol into the ligand framework improves catalysis beyond the addition of phenol to the electrolyte, we investigated the change in linear sweep voltammetry for MnBr(bpy)$(CO)_3$ in the presence of CO_2 and 10 equiv of dissolved phenol. The concentration of proton donor in solution ([H_2O] + [phenol]) was thus 2.78 M. The results are shown in Figure 7 (green trace) against linear

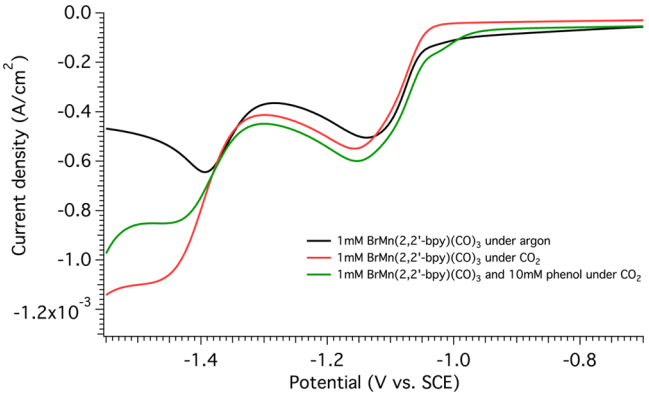

Figure 7. Linear sweep voltammogram of MnBr(2,2′-bipyridine)-$(CO)_3$ under argon (black trace), CO_2 (red trace), and with the presence of 10 mM phenol under CO_2 (green trace) at 100 mV s^{-1} in CH_3CN with 0.1 M tetrabutylammonium perchlorate (TBAP) as the supporting electrolyte and 5% water. The complex was loaded at a concentration of 1 mM.

sweeps for MnBr(bpy)$(CO)_3$ under argon (black trace) and CO_2 (red trace), for reference. At the potential of the first reduction, ca. −1.15 V vs SCE, the three sweeps overlap as expected, indicating that there is limited current enhancement. At the potential of the second reduction, ca. −1.4 V vs SCE, both the green trace (10 mM phenol + CO_2) and red trace (CO_2) show current enhancement relative to the black trace (argon), as a result of the catalytic reduction of CO_2. Importantly, the increase in current density for the green trace is less than that of the red trace—the addition of phenol at this concentration retards the catalytic rate—which further confirms that the current enhancement observed for **1** cannot be achieved solely with the addition of phenol.

As an additional measure, the efficacy of **1** for reducing of CO_2 to CO was measured against **2** and MnBr(bpy)$(CO)_3$ using preparative scale electrolysis at a controlled potential. The electrolysis of each compound was performed under an atmosphere of CO_2 at −1.5 V vs SCE in a solution of CH_3CN/H_2O (5%) and 0.1 M TBAP within a two-compartment cell. The catholyte headspace was sampled and analyzed via GC approximately every 20 min for 4 h (Figure 8). All

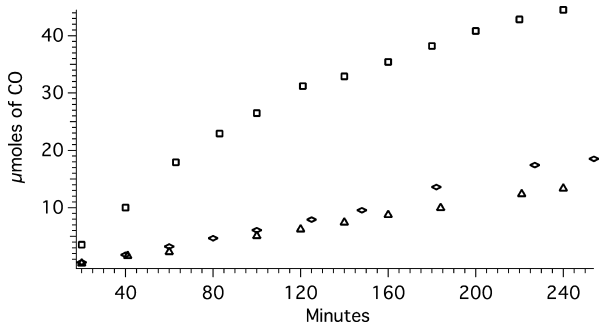

Figure 8. Comparison of the CO_2 reduction activity for MnBr(HOPh-bpy)$(CO)_3$ (□, **1**), MnBr(MeOPh-bpy)$(CO)_3$ (△, **2**), and MnBr-(bpy)$(CO)_3$ (<>) as CO production (*y*-axis, μmol) versus time (*x*-axis, minutes). Data were collected at −1.5 V vs SCE with solutions of the complex (1 mM) loaded in CO_2-saturated CH_3CN with 0.1 M tetrabutylammonium perchlorate (TBAP) as the supporting electrolyte and water (5%).

complexes displayed a short induction period of 20−40 min where Faradaic efficiencies were low, which we ascribe to a latency in the diffusion of CO product from solution into the headspace. During the 4 h experiment, **1** (red squares) produced 44.5 μmol of CO, as mentioned, with an average Faradaic efficiency of 76% and a maximum of 86%. Compound **2** (blue squares) produced less CO (13.3 μmol) but retained a similar Faradaic efficiency to **1**, with a maximum of 83% and an average of 67% over 4 h. Lastly, MnBr(bpy)$(CO)_3$ produced 18.5 μmol of CO, which is a value between that observed for **1** and **2**, and the average Faradaic efficiency was 75%, with a maximum of 100%. Clearly, while the average Faradaic efficiencies are comparable among the three complexes, the high turnover frequency (TOF) of **1** relative to **2** and MnBr(bpy)$(CO)_3$ yields substantially more CO over the 4 h window. [Note: Turnover frequency (TOF) is a term used to evaluate molecular catalysts in homogeneous solution that has been borrowed for the characterization of molecular electrocatalysts. The application of this concept to an electrocatalytic reaction is challenging, because the TOF is potential dependent,[34] with no present consensus on what potential(s) to employ, and published electroanalytical equations for the

DOI: 10.1021/acs.inorgchem.5b00233
Inorg. Chem. 2015, 54, 5285−5294

definition of TOF do not provide similar calculated results. For example, Savéant provides a TOF of 2.0×10^3 s^{-1} for $ReCl(bpy)(CO)_3$. Kubiak has demonstrated that the 4,4′-di*tert*butyl analogue is significantly more active than the parent complex, but reports a TOF of 16 s^{-1}.[12,34] There is a consensus in the literature that the quantity $(i_{cat}/i_p)^2$, obtained from cyclic voltammetry, is proportional to the TOF. In this term, i_{cat} is the limiting current observed in the presence of substrate and i_p is the peak current associated with the catalyst in the absence of substrate. These terms are potential-independent in cases where the catalytic current is measured at its plateau value. Therefore, although reported TOFs are not standardized and, thus, not easily compared, $(i_{cat}/i_p)^2$ values provide useful benchmark of the relative TOF.] Furthermore, the similarity in performance between **2** and $MnBr(bpy)(CO)_3$ suggests that the anisole moiety of **2** is innocent and, because of the lack of a phenolic proton, does not improve catalysis.

A notable feature of **1** is that it displays an increase in relative TOF when compared to the parent complex, $MnBr(bpy)(CO)_3$, and a reduced overpotential for CO_2 reduction. Other modifications of Mn(I)-tricarbonyl catalysts, such as the extension of bpy to 4,4′-di-*tert*-butyl-bpy[12] yield increased current densities at the expense of the overpotential. For comparison, we determined the overpotential and relative TOF of several relevant catalysts, including (i) a modified manganese catalyst, (ii) the analogous Rh(I)-tricarbonyl catalyst with bpy, which is the originally reported CO_2 electrocatalyst in this homologous series, and (iii) an iron-porphyrin catalyst with and without ancillary phenolic groups. These results are shown in Table 1.

Table 1. Overpotentials (η), Current Densities (j), Relative Turnover Frequencies ($(i_{cat}/i_p)^2$), and Peak Potentials in the Absence of a Substrate (E_p) for Selected Catalysts[a]

catalyst	η (mV)	j (mA/cm^2)	$(i_{cat}/i_p)^2$	E_p (V)	source
$ReCl(bpy)(CO)_3$[b]	810	0.5	12	−1.73	ref 21
$MnBr(bpy)(CO)_3$[c]	430	0.5	2.6	−1.40	this work
$MnBr(HOPh\text{-}bpy)(CO)_3$[c]	440	3.1	119	−1.30	this work
$MnBr(MeOPh\text{-}bpy)(CO)_3$[c]	270	0.5	4.4	−1.30	this work
$MnBr(4,4'\text{-di-}tert\text{-butyl-}bpy)(CO)_3$[d]	760	3.5	625	−1.57	ref 12
FeTDMPP[e,f]	1000		625	−2.02	ref 34
FeTDHPP[e,f]	700		3600	−1.57	ref 34

[a]Overpotentials determined using the approach of Appel and Helm,[39] and current densities were determined at the potential of $E_{cat/2}$ (the overpotential, see text). [b]In MeCN with 0.1 M TBAH electrolyte. [c]In MeCN with 0.1 M tetrabutylammonium perchlorate (TBAP) electrolyte and 2.77 M H_2O. [d]In MeCN with 0.1 M tetrabutylammonium hexafluorophosphate (TBAH) electrolyte and 2.9 M MeOH. [e]TDHPP = 5,10,15,20-tetrakis(2′,6′-dihydroxyphenyl)-porphyrin. [f]In DMF with 0.1 M TBAH electrolyte and 2.0 M H_2O.

To calculate the overpotential of each catalyst, we began with the standard potential for the CO_2/CO couple in acetonitrile ($E^\circ_{CO_2}$ = −0.89 V vs SCE), as derived by Savéant and co-workers.[34] Using the approach reported by Appel and Helm, we employed $E_{cat/2}$, the voltage at half of the catalytic current maximum, as the operational electrode potential.[39] This potential is preferred because it is less subjective than the onset potential, and any potential in the plateau region yields the same value for $E_{cat/2}$. The current densities listed in Table 1 were determined at $E_{cat/2}$.

From the values in Table 1, the advantage of employing manganese catalysts relative to the rhenium analogue is clear, since the overpotential for CO_2 reduction halves from $ReCl(bpy)(CO)_3$ to $MnBr(bpy)(CO)_3$, along with a small decrease in relative TOF. Among the manganese catalysts shown, **1** achieves comparable current densities to $MnBr(4,4'\text{-di-}tert\text{-butyl-bpy})(CO)_3$ (3.1 mA/cm^2 vs 3.5 mA/cm^2) with 42% less overpotential (440 mV vs 760 mV). However, there is a tradeoff in this case, since the decreased overpotential is linked to a decrease in the relative TOF by a factor of 5.

As mentioned, phenolic ligands have also been employed in iron-porphyrin compounds These systems have relatively large turnover frequencies. As such, they represent an interesting comparison with the compounds under consideration here. As reported in Table 1, FeTDMPP yields a relative TOF of 625, but requires a large overpotential of 1 V. The addition of six ancillary phenolic groups to the porphyrin structure (FeTDHPP) reduces the overpotential to 700 mV and increases the relative TOF to 3600, a 5-fold improvement. We observe a 46-fold increase in the relative TOF after the addition of a phenolic group to **1** at an overpotential 40% less than that of FeTDHPP. The improvement in FeTDHPP over FeTDMPP has been suggested to originate from higher local proton concentration at the active site. Whether the observed catalyst improvement was due to the proton concentration, or perhaps to the generation of a hydrogen-bonded reactive intermediate was not explored.

THEORY

To further understand and evaluate the nature of the catalytic current enhancement observed for **1**, relative to $MnBr(bpy)(CO)_3$, we examined possible reaction trajectories with theory. Briefly, in related $ReX(N{-}N)(CO)_3$ systems, the reaction pathway for the two-electron reduction of CO_2 to CO is proposed to involve a metallocarboxylic acid intermediate from η^1-CO_2 bonding to the coordinatively unsaturated, reduced intermediate: $[Re(N{-}N)(CO)_3]^-$. The formation of a M−COOH species was originally proposed on the basis of facile and quantitative yields of metallocarboxylates from nucleophilic attack on CO_2 by a variety of reduced-metal centers,[40,41] and the precedence for subsequent O-protonation. These concepts were reviewed by Keene and Sullivan in 1993.[42]

Later, Gibson and co-workers synthesized $Re(N{-}N)(CO)_3COOH$ and observed the production of CO after adding it to a CO_2-saturated solvent. A transient rhenium-tetracarbonyl complex, $[Re(N{-}N)(CO)_4]^+$ was postulated to be the source of evolved CO.[43−45] In a 2009 review, Morris, Meyer, and Fujita included the formation of $Re(N{-}N)(CO)_3COOH$ and $[Re(N{-}N)(CO)_4]^+$ in a proposed scheme for the reduction of CO_2 to CO.[46] Moreover, in subsequent work, we suggested that the interaction of an additional CO_2 molecule with $Re(N{-}N)(CO)_3COOH$ could mediate removal of the hydroxyl group as bicarbonate on the basis of theory and isotope labeling experiments.[47] More recently, Keith et al. expounded the pathway further by examining intermediates of the reaction with theory to predict the redox potential and pK_a for the species involved. They concluded that removal of the hydroxyl group from $Re(N{-}N)(CO)_3COOH$ is the rate-limiting step (i.e., C−O bond cleavage) and that $[Re(N{-}N)(CO)_4]^+$ is the CO generating species.[48]

DOI: 10.1021/acs.inorgchem.5b00233
Inorg. Chem. 2015, 54, 5285−5294

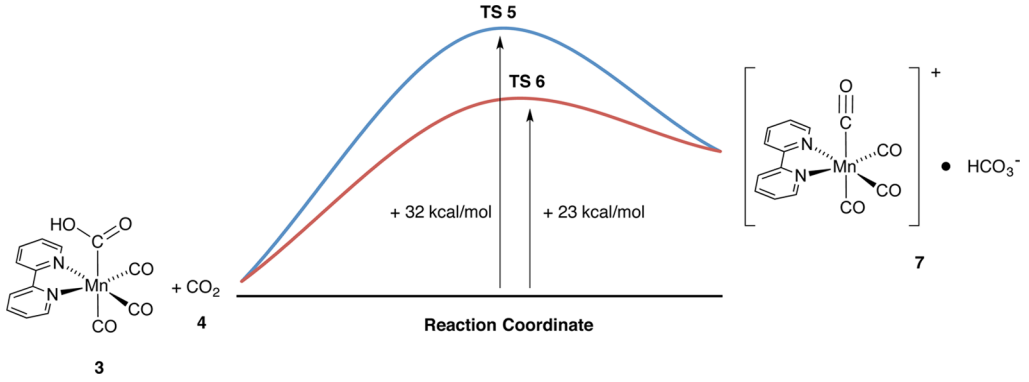

Figure 9. Standard free-energy profile for the reaction of $Mn(bpy)(CO)_3COOH$ (**3**) with CO_2 (**4**). Two potential pathways exist: a lower-energy path, where the C atom of CO_2 interacts with the carbonyl of Mn−COOH (**TS 6**), and a higher-energy path, where the same C atom interacts with the alcohol instead (**TS 5**). In either case, a $Mn(bpy)(CO)_4^+$–HCO_3^- adduct (**7**) results.

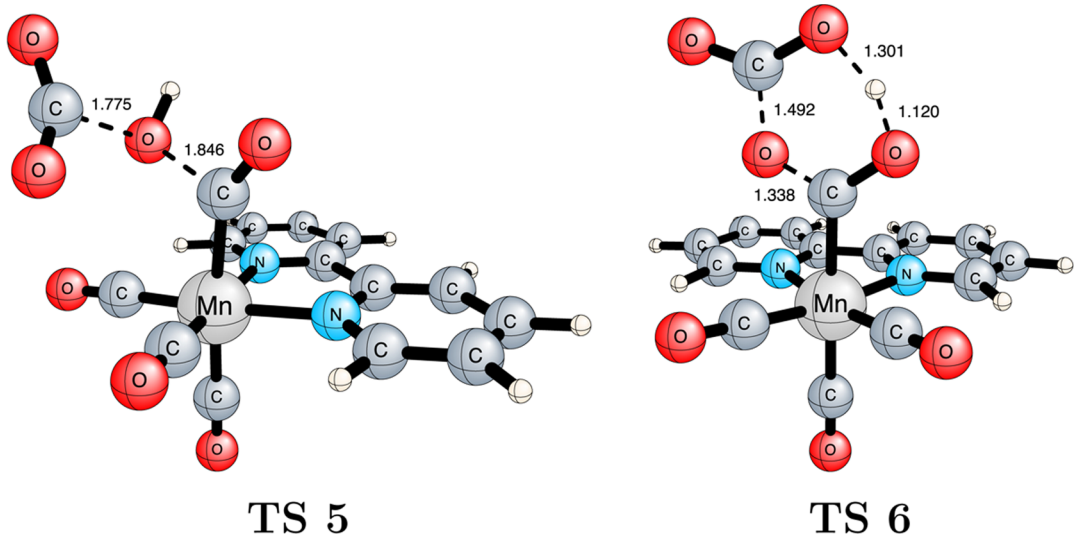

Figure 10. Optimized geometries of **TS 5** and **TS 6** for the interaction of a molecule of CO_2 (**4**) with $Mn(bpy)(CO)_3COOH$ (**3**). Bond lengths are shown in Angstroms.

Given this insight, we postulated that the rate-limiting step for the manganese analogue mirrored that of rhenium for the two-electron pathway. Recent work by Kubiak and co-workers supports this assertion. They reported that, on the basis of cyclic voltammetry and infrared spectroelectrochemistry investigations, a $[Mn(bpy)(CO)_3]^-$ intermediate serves as the active species for CO_2 reduction with manganese, which is analogous to the proposed pathway for rhenium.[37] Accordingly, we truncated the potential energy surface and considered only the transformation of

$$Mn(N{-}N)(CO)_3COOH + A \rightarrow [Mn(N{-}N)(CO)_4]^+ + B$$

as a barometer for improved design. Our theoretical investigation began by considering $Mn(bpy)(CO)_3COOH$ in a CO_2-saturated acetonitrile environment. Following our previous work with rhenium,[47] we probed the interaction of an additional molecule of CO_2 with this species to yield bicarbonate and the necessary tetracarbonyl intermediate. Two possible pathways were identified, as shown in Figure 9, from the separate interaction of CO_2 with the two O atoms of the carboxylic acid ligand.

In the higher-energy route, free CO_2 (**4**) interacts with the O atom of the hydroxyl group through C−O bond formation (see Figure 10). Subsequent cleavage of the adjacent C−O bond between the carbonyl and hydroxyl constituents of the carboxylic acid ligand yields the tetracarbonyl-bicarbonate ion pair, **7**, through **TS 5**. The free energy for this transition state ($\Delta G^{\ddagger}$) is 32.4 kcal mol^{-1} above the reactants (**3** + **4**), and the reaction is overall endergonic (+16.8 kcal mol^{-1}). An alternative, lower-energy path exists ($\Delta G^{\ddagger}$ = 23.0 kcal mol^{-1}) that is proton-assisted. In that case, CO_2 interacts with the O atom of the carbonyl group and the proton of the hydroxyl moiety. Concerted proton transfer occurs as a C−O bond forms between CO_2 and the carbonyl. Following the intrinsic reaction coordinate, we find that the formation of the ion-pair product (**7**) for this route follows from spontaneous decomposition (ΔG = −3.4 kcal mol^{-1}) of the C−O bond between the carbonyl and hydroxyl constituents. We note that the overall free energy to **7** (+16.8 kcal mol^{-1}) is reduced to +11.2 kcal mol^{-1} if the ion pair can overcome electrostatic interactions and dissociate into $Mn(bpy)(CO)_4^+$ and HCO_3^- as solvated ions in solution.

One of the important features of the truncated potential energy surface shown in Figure 9 is the sensitivity of the transition state energies [$\Delta G^{\ddagger}$(**TS 5**), $\Delta G^{\ddagger}$(**TS 6**)] to the

DOI: 10.1021/acs.inorgchem.5b00233
Inorg. Chem. 2015, 54, 5285−5294

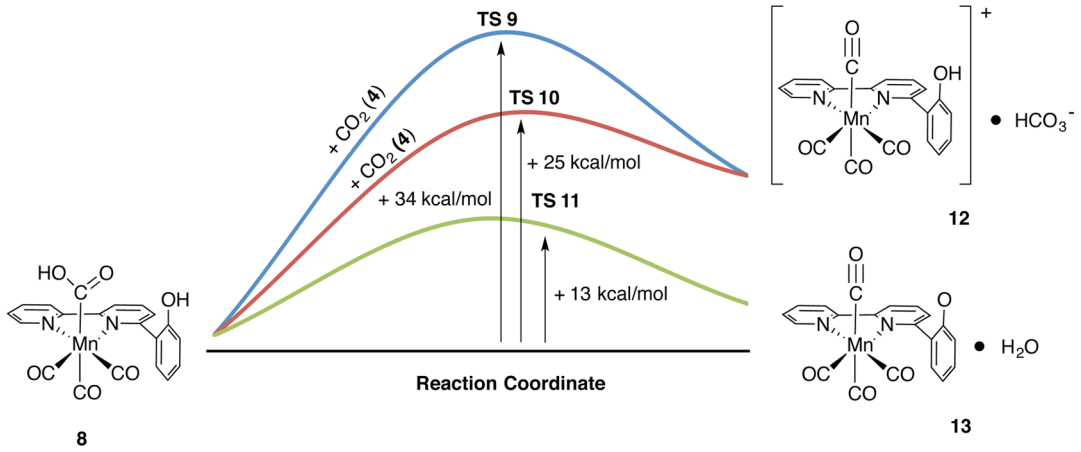

Figure 11. Standard free-energy profile for the reaction of Mn(HOPh-bpy)$(CO)_3$COOH (**8**) with CO_2 (**4**) or the phenolic proton. Three potential pathways exist: a lower-energy path involving proton-assisted dehydration to **13** via **TS 11**, and two paths involving interaction with CO_2 to yield **12**. The latter two routes include a higher-energy path, where the C atom of CO_2 interacts with the alcohol group (through **TS 9**), and a lower-energy path, where the same C atom interacts with the O atom of the carbonyl group within M−COOH (through **TS 10**).

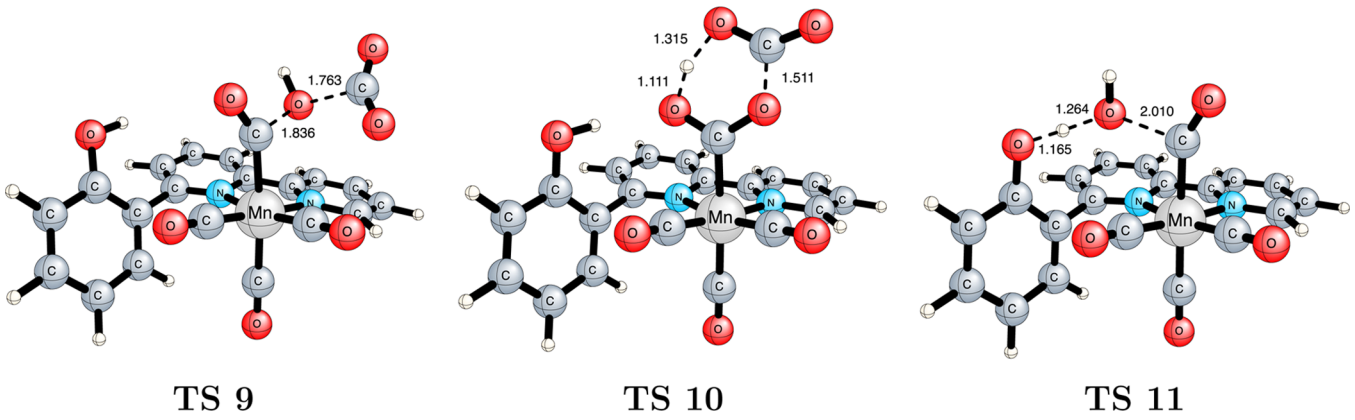

Figure 12. Optimized geometries of **TS 9**, **TS 10**, and **TS 11**. Bond lengths are shown in Angstroms.

entropic corrections from the vibrational, rotational, and translational partition functions. For **TS 5**, the 9.3 kcal mol^{-1} difference between the standard free energy ($\Delta G^{\ddagger}$ = 32.4 kcal mol^{-1}) and the standard enthalpy ($\Delta H^{\ddagger}$ = 23.0 kcal mol^{-1}) is the result of a −5.3 kcal mol^{-1} correction for increased vibrational entropy in the product, a +3.6 kcal mol^{-1} correction for decreased rotational entropy, and a +11.0 kcal mol^{-1} correction for decreased translational entropy. We note that the correction for translational entropy should be interpreted as an upper limit, because, under true reaction conditions, CO_2 is present in excess. Based on this analysis, we conclude that the transition-state free energy will be plagued with this correction as long as another small molecule is used to mediate removal of the hydroxyl group from **4**, since it will have significant translational and rotational entropy. Therefore, we sought to investigate whether the phenolic proton present in **1** allows for an intramolecular reaction to produce the tetracarbonyl intermediate, thereby reducing the entropic penalty significantly.

As with **3**, we began by probing the reactivity of **8**, which includes a pendant phenol, with CO_2. Figure 11 shows a depiction of our results, and graphical representations of the relevant transition state structures are shown in Figure 12. We find that two potential pathways exist for the interaction of CO_2 with **8**, analogous to the same reactivity with **3**. The free-energy barrier for the transition states involved in these two routes resides 34.1 kcal mol^{-1} (**TS 9**) and 24.8 kcal mol^{-1} (**TS 10**) above the reactants [**8** + CO_2 (**4**)], respectively. Compared to the analogous transition states in Figure 9, **TS 9** is 1.7 kcal mol^{-1} higher than that of **TS 5** and **TS 10** is 1.7 kcal mol^{-1} higher than that of **TS 6**. Both reactions are overall endergonic (+18.2 kcal mol^{-1}) to the ion-pair product (**12**).

Importantly, we find a new, lower-energy pathway for intramolecular protonation and subsequent dehydration of the carboxylic acid ligand. This route, through **TS 11**, constitutes a new trajectory and a different product (**13**). Notably, **TS 11** lies 13 kcal mol^{-1} above **8**; 11.4 kcal mol^{-1} below the lowest-energy transition state proposed for hydroxyl removal through reaction with CO_2. The standard enthalpy for **TS 11** differs by only 0.2 kcal mol^{-1} from the free energy, a result of the small loss of vibrational entropy in the product and no change in translational or rotational entropy between **8** and the transition state. The overall reaction to a hydrated tetracarbonyl adduct (**13**) is endergonic (+3.6 kcal mol^{-1}). As previously mentioned, we employed the reactivity of CO_2 as a metric to gauge the improvement from intramolecular protonation, but caution that alternative pathways involving electrolytes, added water, or impurities may exist. To this end, we have evaluated a reaction pathway comparable to **TS 9**, in which a water molecule is substituted for free CO_2, and we have determined that this has an insignificant effect on the reaction barrier free energy (see page S39 in the Supporting Information). Thus, our calculated

DOI: 10.1021/acs.inorgchem.5b00233
Inorg. Chem. 2015, 54, 5285−5294

reaction barriers are insensitive to whether the C atom in CO_2 or a H atom in water is the oxygen acceptor, and our conclusions hold in either case.

SUMMARY

We have demonstrated the design of a catalytic active site for Mn(I)-tricarbonyl catalysts that utilizes a phenolic group in the second coordination sphere. This framework allows for the stabilization of a Mn−CO_2 adduct via hydrogen bonding between the phenolic proton and an O atom of CO_2. Our new catalyst displays over seven times the catalytic current density of MnBr(bpy)$(CO)_3$ at roughly the same overpotential. Moreover, we observe Faradaic efficiencies of up to 86%, with an average efficiency of 76% over 4 h. Using theory, we suggest that the origin of the increased activity observed is the result of an intramolecular mechanism for proton-assisted dehydration of Mn(6-(2-hydroxyphenyl)-bpy)$(CO)_3$COOH. This intramolecular mechanism possesses a lower activation barrier, compared to related trajectories involving free molecules in solution, partially because of the limited entropic penalty of an intramolecular process. Future work will focus on understanding the effect of hydrogen bond geometry and acidity on the reaction of our reduced catalysts with CO_2, as well as the application of these design principles to other CO_2 reduction electrocatalysts.

EXPERIMENTAL METHODS

General Procedures. All electrochemical experiments and bulk electrolyses were performed under air free conditions, unless noted otherwise. Manganese complexes were handled under a red light at all times except during weighing. For all electrochemical experiments, the electrolyte was bubbled with the desired gas (argon or CO_2) for 15 min prior to taking a background scan to ensure a featureless background from 0 to −2.0 V vs SCE. After adding the desired complex, the electrolyte was bubbled for 5 more minutes before collecting experimental data. Complexes were loaded at a concentration of 1 mM for both voltammetry and bulk electrolyses. The total volume of electrolyte used for these experiments was 15 mL for voltammetry and 20 mL for bulk electrolysis. Bulk electrolyses were operated for ∼4 h, and the headspace was analyzed by GC approximately every 20 min. Voltammograms were referenced to ferrocene/ferrocenium at the end of the experiment and then later converted to vs SCE by adding 380 mV.[49] The proton concentration was kept consistent for argon and CO_2 trials by using pH-adjusted water ($HClO_4$) in the case of argon and neutral water in the case of CO_2. Elemental microanalyses were performed at Robertson Microlit Laboratories (Ledgewood, NJ).

Materials. Tetrabutylammonium perchlorate (TBAP) was synthesized by the dropwise addition concentrated perchloric acid into an equimolar solution of tetrabutylammonium bromide in water. The precipitated TBAP was collected, recrystallized three times from ethyl acetate/hexanes, and dried under reduced pressure (<0.1 Torr) for several hours over P_2O_5. Manganese pentacarbonyl bromide (Strem) and 2,2′-bipyridine (Sigma−Aldrich) were used as received. Acetonitrile was bubble degassed and passed through two columns of activated alumina prior to use. Electrolyte solutions were prepared by dissolving TBAP in acetonitrile and passing the solution through a column of activated alumina in a fritted Schlenk filter directly into a Schlenk flask. The electrolyte was stored under an inert atmosphere and bubble degassed immediately before performing any experiments. A 3 mm glassy carbon disk working electrode and a Ag/AgCl reference electrode (BASi Models MF-2012 and MF-2052, respectively) were used in all electrochemical experiments. A platinum mesh (∼1 cm^2) connected to a platinum wire was used as the counter electrode in all electrochemical experiments. A 15 mL three-neck round-bottom flask was used as the electrochemical cell for voltammetry and a 25 mL three-neck round-bottomed flask was used for bulk electrolysis. The working and reference electrodes were secured using "mini" No. 7 Ace-threaded adaptors from Ace-glass. The counter electrode was threaded through a septum, which was then fitted onto one neck of the cell.

Instrumentation. Electrochemical measurements were performed on a Model CHI 760D electrochemical workstation (CH Instruments, Austin, TX). Nuclear magnetic resonance (NMR) spectra were recorded on a Bruker AVANCE spectrometer (500 MHz for ^{1}H nuclei and 125 MHz for ^{13}C nuclei). Chemical shifts are reported in parts per million (ppm) downfield of tetramethylsilane and are referenced to the solvent residual peak. Fourier transform infrared (FT-IR) spectra were recorded on a Nicolet Model 730 FT-IR spectrometer for gas samples and a Nicolet Model 6700 FT-IR spectrometer equipped with a single-reflection diamond ATR attachment for solid samples. Ultraviolet−visible (UV-vis) spectra were recorded on a Hewlett−Packard Model 8453 spectrophotometer. X-ray diffraction (XRD) data were collected with a Bruker Photon 100 CMOS detector using Cu Kα radiation (**1**) or a Bruker Apex II CCD detector using Mo Kα radiation (**2**). CO production was analyzed using a Model HP 5980 GC system with a TCD analyzer and analog integrator. An Agilent Model CP7538 molecular sieve column was used to separate CO from CO_2 at a column head pressure of 12 psi, an oven temperature of 70 °C, an injection temperature of 200 °C, and a detector temperature of 250 °C.

Preparation of 1. An aliquot of $MnBr(CO)_5$ (49.8 mg, 0.181 mmol) was added to 6-(2-hydroxyphenyl)-bpy (45 mg, 0.181 mmol) that had been dissolved in 15 mL of degassed MeOH. The resulting orange solution was heated to reflux for 2 h under argon, then allowed to cool to room temperature before filtration. The filtrate was collected and concentrated, then washed with Et_2O and dried *in vacuo* to afford 69.6 mg (82% yield) of orange product. The following were observed for the mixture of atropisomers (hydroxyphenyl adduct parallel and antiparallel to the axial plane): IR ν_{CO} (ATR, cm^{-1}): 2019 (s), 1920 (br). ^{1}H NMR (DMSO-d_6, 500 MHz): δ 9.99−9.92 (1H, s), 9.34−9.12. (1 H, m), 8.90−8.56 (2 H, m), 8.45−8.16 (2 H, m), 7.91−7.55 (2 H, m) 7.52−7.20 (2 H, m) 7.18−6.92 (2 H, m). ^{13}C NMR (DMSO-d_6, 125 MHz): δ 224.29, 222.86, 221.42, 221.35, 217.50, 216.27, 162.79, 162.48, 157.53, 156.95, 156.47, 155.45, 155.43, 154.97, 153.34, 153.28, 139.49, 139.43, 139.36, 138.41, 131.58, 131.52, 131.43, 130.90, 130.12, 128.79, 126.85, 126.33, 124.00, 123.94, 121.98, 121.81, 119.32, 118.84, 116.79, 115.87. Anal. Found: C, 48.80; H, 2.52; N, 5.91. Calcd: C, 48.85; H, 2.59; N, 6.00.

Preparation of 2. An aliquot of $MnBr(CO)_5$ (171.8 mg, 0.625 mmol) was added to 6-(2-methoxyphenyl)-bpy (164 mg, 0.625 mmol) that had been dissolved in 30 mL of degassed MeOH. The resulting orange solution was heated to reflux for 2 h under argon, then allowed to cool to room temperature before filtration. The filtrate was collected and concentrated, then washed with Et_2O and dried *in vacuo* to afford 296 mg (98% yield) of orange product. The following were observed for the mixture of atropisomers (methoxyphenyl adduct parallel and antiparallel to the axial plane): IR ν_{CO} (ATR, cm^{-1}): 2021 (s), 1934 (s), 1882 (s). ^{1}H NMR (DMSO-d_6, 500 MHz): δ 9.25−9.20 (1 H, m), 8.75−8.50 (2 H, m), 8.37−8.15 (2 H, m), 7.84−7.45 (3 H, m), 7.45−7.10 (3 H, m), 3.87−3.72 (3 H, s). ^{13}C NMR (DMSO-d_6, 125 MHz): δ 224.71, 223.19, 221.92, 218.29, 216.87, 162.71, 162.52, 157.89, 157.41, 157.02, 156.13, 153.99, 153.98, 140.19, 132.60, 131.99, 131.82, 131.38, 129.26, 127.53, 124.77, 122.83, 121.54, 111.98, 57.16, 56.10. Anal. Found: C, 49.93; H, 2.81; N, 5.74. Calcd: C, 49.92; H, 2.93; N, 5.82.

THEORETICAL METHODS

Optimized geometric structures and vibrational frequencies were obtained from density functional theory (DFT) computations as implemented in Gaussian 09.[50] Computations were performed with the inclusion of an implicit solvent model (CPCM)[51,52] using the default parameters for acetonitrile (ϵ = 35.688). Stationary points were verified with frequency analysis using analytic second derivatives, and transition-state structures

DOI: 10.1021/acs.inorgchem.5b00233
Inorg. Chem. 2015, 54, 5285−5294

were connected to minima using intrinsic reaction coordinate (IRC) computations.[53−55] Tight convergence (RMS force ≤1 × $10^{-5} E_h a_0^{-1}$) and an ultrafine grid (99 radial shells, 590 angular points per shell) were employed throughout. Aligned with our prior work,[20,47] we employed the M06-L local density functional developed by Zhao and Truhlar.[56] Mn atoms were parametrized with LANL08F.[57] This Los Alamos basis set includes a Hay−Wadt effective core potential (ECP)[58] and an uncontracted, triple-ζ description of the valence orbitals. The "light" atoms (H, C, N, and O) were described by the 6-31++G(d,p) Pople basis set.[59,60]

■ ASSOCIATED CONTENT

Supporting Information

The Supporting Information is available free of charge on the ACS Publications website at DOI: 10.1021/acs.inorgchem.5b00233.

■ AUTHOR INFORMATION

Corresponding Author

*E-mail: bocarsly@princeton.edu.

Author Contributions

§These authors contributed equally to this work.

Notes

The authors declare no competing financial interest.

■ ACKNOWLEDGMENTS

Work at Princeton was supported by funding from the DOD-MURI Program under AFOSR Award No. FA9550-10-1-057 and the National Science Foundation under Grant No. CHE-1308652. T.W.S. acknowledges the National Science Foundation for a graduate research fellowship. Research at the University of Georgia was supported by the National Science Foundation (Grant Nos. CHE-1054286 and CHE-1361178).

■ REFERENCES

(1) Kondratenko, E. V.; Mul, G.; Baltrusaitis, J.; Larrazábal, G. O.; Pérez-Ramírez, J. *Energy Environ. Sci.* **2013**, *6*, 3112−3135.
(2) Hara, K.; Kudo, A.; Sakata, T. *J. Electroanal. Chem.* **1995**, *391*, 141−147.
(3) Chen, Y.; Kanan, M. W. *J. Am. Chem. Soc.* **2012**, *134*, 1986−1989.
(4) Medina-Ramos, J.; DiMeglio, J. L.; Rosenthal, J. *J. Am. Chem. Soc.* **2014**, *136*, 8361−8367.
(5) Cokoja, M.; Bruckmeier, C.; Reiger, B.; Herrmann, W. A.; Kühn, F. E. *Angew. Chem., Int. Ed.* **2011**, *50*, 8510−8537.
(6) Savéant, J.-M. *Chem. Rev.* **2008**, *108*, 2348−2378.
(7) Fujita, E.; Brunschwig, B. S.; Ogata, T.; Yanagida, S. *Coord. Chem. Rev.* **1994**, *132*, 195−200.
(8) Costentin, C.; Robert, M.; Savéant, J.-M. *Chem. Soc. Rev.* **2013**, *42*, 2423−2436.
(9) Schneider, J.; Jia, H.; Muckerman, J. T.; Fujita, E. *Chem. Soc. Rev.* **2012**, *41*, 2036−2051.
(10) Benson, E. E.; Kubiak, C. P.; Sathrum, A. J.; Smieja, J. M. *Chem. Soc. Rev.* **2009**, *38*, 89−99.
(11) Bourrez, M.; Molton, F.; Chardon-Noblat, S.; Deronzier, A. *Angew. Chem., Int. Ed.* **2011**, *50*, 9903−9906.
(12) Smieja, J. M.; Sampson, M. D.; Grice, K. A.; Benson, E. E.; Froehlich, J. D.; Kubiak, C. P. *Inorg. Chem.* **2013**, *52*, 2484−2491.
(13) Bourrez, M.; Orio, M.; Molton, F.; Vezin, H.; Duboc, C.; Deronzier, A.; Chardon-Noblat, S. *Angew. Chem., Int. Ed.* **2013**, *53*, 240−243.
(14) Takeda, H.; Koizumi, H.; Okamoto, K.; Ishitani, O. *Chem. Commun.* **2014**, *50*, 1491−1493.
(15) Compain, J.-D.; Bourrez, M.; Haukka, M.; Deronzier, A.; Chardon-Noblat, S. *Chem. Commun.* **2014**, *50*, 2539−2542.
(16) Sampson, M. D.; Nguyen, A. D.; Grice, K. A.; Moore, C. E.; Rheingold, A. L.; Kubiak, C. P. *J. Am. Chem. Soc.* **2014**, *136*, 5460−5471.
(17) Agarwal, J.; Shaw, T. W.; Stanton, C. J.; Majetich, G. F.; Bocarsly, A. B.; Schaefer, H. F. *Angew. Chem., Int. Ed.* **2014**, *53*, 5152−5155.
(18) Ishitani, O.; George, M. W.; Ibusuki, T.; Johnson, F. P. A.; Koike, K.; Nozaki, K.; Pac, C. J.; Turner, J. J.; Westwell, J. R. *Inorg. Chem.* **1994**, *33*, 4712−4717.
(19) Hori, H.; Johnson, F. P. A.; Koike, K.; Ishitani, O.; Ibusuki, T. *J. Photochem. Photobiol. A* **1996**, *96*, 171−174.
(20) Agarwal, J.; Fujita, E.; Schaefer, H. F.; Muckerman, J. T. *J. Am. Chem. Soc.* **2012**, *134*, 5180−5186.
(21) Smieja, J. M.; Kubiak, C. P. *Inorg. Chem.* **2010**, *49*, 9283−9289.
(22) Kutal, C.; Weber, M. A.; Ferraudi, G.; Geiger, D. *Organometallics* **1985**, *4*, 2161−2166.
(23) Kutal, C.; Corbin, A. J.; Ferraudi, G. *Organometallics* **1987**, *6*, 553−557.
(24) Hayashi, Y.; Kita, S.; Brunschwig, B.; Fujita, E. *J. Am. Chem. Soc.* **2003**, *125*, 11976−11987.
(25) Sullivan, B. P.; Bolinger, C. M.; Conrad, D.; Vining, W. J.; Meyer, T. J. *J. Chem. Soc. Chem. Commun.* **1985**, 1414−1415.
(26) Wong, K.-Y.; Chung, W.-H.; Lau, C.-P. *J. Electroanal. Chem.* **1998**, *453*, 161−169.
(27) Bhugun, I.; Lexa, D.; Savéant, J.-M. *J. Am. Chem. Soc.* **1994**, *116*, 5015−5016.
(28) Bhugun, I.; Lexa, D.; Savéant, J.-M. *J. Am. Chem. Soc.* **1996**, *118*, 1769−1776.
(29) DuBois, D. L. *Inorg. Chem.* **2014**, *53*, 3935−3960.
(30) Carver, C. T.; Matson, B. D.; Mayer, J. M. *J. Am. Chem. Soc.* **2012**, *134*, 5444−5447.
(31) Miedaner, A.; Noll, B. C.; DuBois, D. L. *Organometallics* **1997**, *16*, 5779−5791.
(32) Steffey, B. D.; Curtis, C. J.; DuBois, D. L. *Organometallics* **1995**, *14*, 4937−4943.
(33) Jeoung, J.-H.; Dobbek, H. *Science* **2007**, *318*, 1461−1464.
(34) Costentin, C.; Drouet, S.; Robert, M.; Savéant, J.-M. *Science* **2012**, *338*, 90−94.
(35) Costentin, C.; Passard, G.; Robert, M.; Savéant, J.-M. *J. Am. Chem. Soc.* **2014**, *136*, 11821−11829.
(36) Jeffrey, J. C.; Schatz, E.; Ward, M. D. *J. Chem. Soc., Dalton Trans.* **1992**, *12*, 1921−1928.
(37) Machan, C. W.; Sampson, M. D.; Chabolla, S. A.; Dang, T.; Kubiak, C. P. *Organometallics* **2014**, *33*, 4550−4559.
(38) Nicholson, R. S.; Shain, I. *Anal. Chem.* **1964**, *36*, 706−723.
(39) Appel, A. M.; Helm, M. L. *ACS Catal.* **2014**, *4*, 630−633.
(40) Cutler, A. R.; Hanna, P. K.; Vites, J. C. *Chem. Rev.* **1988**, *88*, 1363−1403.
(41) Angelici, R. J. *Acc. Chem. Res.* **1972**, *5*, 335−341.
(42) Keene, F. R., Sullivan, B. P. *Electrochemical and Electrocatalytic Reactions of Carbon Dioxide*; Sullivan, B. P., Krist, K., Guard, H. E., Eds.; Elsevier: Amsterdam, 1993.
(43) Gibson, D. H.; Yin, X. *J. Am. Chem. Soc.* **1998**, *120*, 11200−11201.
(44) Gibson, D. H.; Yin, X. *Chem. Commun.* **1999**, 1411−1412.
(45) Gibson, D. H.; Yin, X. L.; He, H. Y.; Mashuta, M. S. *Organometallics* **2003**, *22*, 337−346.
(46) Morris, A. J.; Meyer, G. J.; Fujita, E. *Acc. Chem. Res.* **2009**, *42*, 1983−1994.
(47) Agarwal, J.; Sanders, B. C.; Fujita, E.; Schaefer, H. F.; Harrop, T. C.; Muckerman, J. T. *Chem. Commun.* **2012**, *48*, 6797−6799.
(48) Keith, J. A.; Grice, K. A.; Kubiak, C. P.; Carter, E. A. *J. Am. Chem. Soc.* **2013**, *135*, 15823−15829.
(49) Connelly, N. G.; Geiger, W. E. *Chem. Rev.* **1996**, *96*, 877−910.
(50) Frisch, M. J. et al. *Gaussian 09, Revision B.01*; Gaussian, Inc.: Wallingford, CT, 2009.
(51) Barone, V.; Cossi, M. *J. Phys. Chem. A* **1998**, *102*, 1995−2001.
(52) Cossi, M.; Rega, N.; Scalmani, G.; Barone, V. *J. Comput. Chem.* **2003**, *24*, 669−681.

DOI: 10.1021/acs.inorgchem.5b00233
Inorg. Chem. 2015, 54, 5285−5294

(53) Fukui, K. *Acc. Chem. Res.* **1981**, *14*, 363−368.
(54) Hratchian, H. P.; Schlegel, H. B. *J. Chem. Phys.* **2004**, *120*, 9918−9924.
(55) Hratchian, H. P.; Schlegel, H. B. *J. Chem. Theory and Comput* **2005**, *1*, 61−69.
(56) Zhao, Y.; Truhlar, D. G. *J. Chem. Phys.* **2006**, *125*, 194101.
(57) Roy, L. E.; Hay, P. J.; Martin, R. L. *J. Chem. Theory Comput.* **2008**, *4*, 1029−1031.
(58) Wadt, W. R.; Hay, P. J. *J. Chem. Phys.* **1985**, *82*, 284−298.
(59) Dill, J. D.; Pople, J. A. *J. Chem. Phys.* **1975**, *62*, 2921−2923.
(60) Francl, M. M.; Pietro, W. J.; Hehre, W. J.; Binkley, J. S.; Gordon, M. S.; Defrees, D. J.; Pople, J. A. *J. Chem. Phys.* **1982**, *77*, 3654−3665.

DOI: 10.1021/acs.inorgchem.5b00233
Inorg. Chem. 2015, 54, 5285−5294